8368 J. Med. Chem. 2010, 53, 8368–8375
DOI: 10.1021/jm100825h

Journal of Medicinal Chemistry Article

Design, Synthesis, and Structure−Activity Relationships of 3-Ethynyl-1*H*-indazoles as Inhibitors of the Phosphatidylinositol 3-Kinase Signaling Pathway

Elisa Barile,[†,§] Surya K. De,[†,§] Coby B. Carlson,[‡] Vida Chen,[†] Christine Knutzen,[†] Megan Riel-Mehan,[†] Li Yang,[†] Russell Dahl,[†] Gary Chiang,[†] and Maurizio Pellecchia*[,†]

[†]*Sanford-Burnham Medical Research Institute, La Jolla, California 92037, United States, and* [‡]*Invitrogen Discovery Assays and Services (Now a Part of Life Technologies), 501 Charmany Drive, Madison, Wisconsin 53719, United States.* [§]*These authors contributed equally to this work*

Received July 2, 2010

A new series of 3-ethynyl-1*H*-indazoles has been synthesized and evaluated in both biochemical and cell-based assays as potential kinase inhibitors. Interestingly, a selected group of compounds identified from this series exhibited low micromolar inhibition against critical components of the PI3K pathway, targeting PI3K, PDK1, and mTOR kinases. A combination of computational modeling and structure−activity relationship studies reveals a possible novel mode for PI3K inhibition, resulting in a PI3Kα isoform-specific compound. Hence, by targeting the most oncogenic mutant isoform of PI3K, the compound displays antiproliferative activity both in monolayer human cancer cell cultures and in three-dimensional tumor models. Because of its favorable physicochemical, *in vitro* ADME and drug-like properties, we propose that this novel ATP mimetic scaffold could prove useful in deriving novel selecting and multikinase inhibitors for clinical use.

Introduction

The PI3K/AKT/mTOR[a] cascade is an important cellular signaling pathway that regulates intersecting biological processes such as cell growth and proliferation, cell survival, protein synthesis, and glycolysis metabolism.[1−3] Physiological stimulation of this cascade occurs through the binding of growth factors (e.g., insulin or insulin-like growth factor; IGF-1) to receptor tyrosine kinases (RTK) on the cell surface. Subsequent activation of the lipid phosphatidylinositol 3-kinase (PI3K) leads to the phosphorylation of phosphatidylinositol 4,5-bisphosphate (PIP_2) to produce phosphatidylinositol 3,4,5-triphosphate (PIP_3), which in turn interacts with the pleckstrin homology (PH) domain of AKT and recruits the kinase to the plasma membrane. Full activation of AKT requires phosphorylation of two distinct residues: Thr308 by the upstream kinase PDK1 and Ser473 by the mammalian target of rapamycin complex 2 (mTORC2).[1−3] Activated AKT, among its wide array of downstream effects, increases protein synthesis rate by phosphorylation at Thr246 of the proline-rich substrate of 40 kDa (PRAS40). This substrate is further regulated through phosphorylation at Ser183 by the mTOR complex 1 (mTORC1). Downstream of mTORC1, signaling events can go through p70 S6 kinase (S6K1), which in turn phosphorylates the programmed cell death protein (PDCD4) at residue Ser457 (Figure 1).

Because of its involvement in a variety of cellular events, such as survival, proliferation, cell motility, and invasion,[4] hyperactivation of the PI3K signaling pathway is one of the most common molecular events in nearly every form of human cancer.[5−8] Indeed, aberrant activation of the PI3K cascade, including PTEN inactivation and PI3K activating mutations, is present in about 32% of colon cancers, 30% of breast cancers, 30% of melanomas,[9] 27% of brain cancers, and 25% of stomach cancers.[10,11] It is for these reasons that considerable drug discovery efforts are ongoing, targeting several components of this signaling cascade using either single and multiple target strategies.[12−16] Interestingly, clinical data suggest that multikinase inhibitors (MKIs) produce greater benefit over single kinase inhibition, especially in solid tumors where different kinases and different pathways synergistically contribute to tumor proliferation.[17−19] Indeed, emerging phase II clinical trial data reveal that dual PI3K/mTOR inhibitors may be more effective, having the advantage of being less susceptible to PI3K drug resistance owing to their preserved activity against mTOR.[16]

In our drug discovery program we interrogated the PI3K signaling pathway, and we report on the identification of a novel scaffold of the 3-ethynylindazole family as multiple PI3K/PDK1/mTOR inhibitors. Such scaffold represents a novel lead structure for the PI3K pathway, suitable for further functionalization and drug development.

Results and Discussion

Compounds **6**−**19** (Table 1) were prepared as shown in Scheme 1. Compound **1** was iodinated, and Boc protection was performed according to the previously reported procedures.[20] Compound **3** (Scheme 1) was coupled with the appropriate alkyne using the Sonogashira reaction conditions

*Corresponding author. E-mail: mpellecchia@sanfordburnham.org. Phone: 858-646-3159. Fax: 858-713-9925.

[a] Abbreviations: PI3K, phosphatidylinositol 3-kinase; PDK1, 3-phosphoinositide-dependent protein kinase-1; RTK, receptor tyrosine kinases; AKT, protein kinase B; mTOR, mammalian target of rapamycin; PTEN, phosphatase and tensin homologue protein; PIP2, phosphatidylinositol 4,5-bisphosphate; PIP3, phosphatidylinositol 3,4,5-triphosphate; PDCD4, programmed cell death protein; S6K1, S6 kinase β-1; GFP, green fluorescent protein.

 Published on Web 11/09/2010

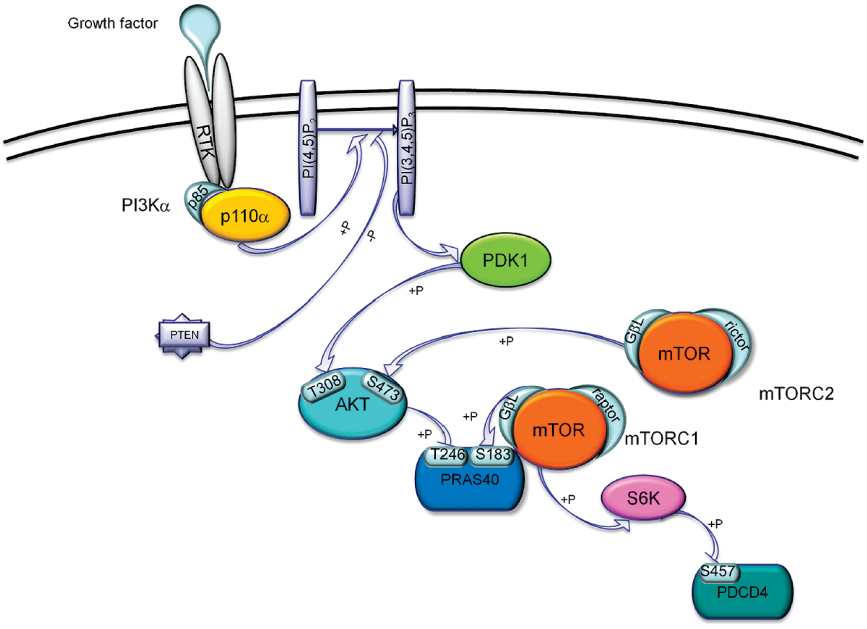

Figure 1. Schematic representation of the PI3K/mTOR signaling pathway highlighting the phosphorylation sites tested in our cellular and biochemical assays.

to give **4** and its analogues in moderate yield (45−65%). Compound **4** was treated with TFA to afford the final compound **5** and its analogues (**6**−**19**, Table 1) in good yields (89−95%). Similarly, compounds **20** and **21** (Table 1) were synthesized starting from 7-azaindazole instead of indazole and following the same synthetic procedure reported in Scheme 1 for indazole derivatives.

We chose to initially screen the synthesized compounds (shown in Table 1) in a cell-based format using a LanthaScreen cellular assay technology, recently reported and successfully applied to the analysis of the PI3K/AKT/mTOR pathway.[21−23] This assay platform uses individual cell lines that stably express key kinase substrate within the cascade as GFP-fusion proteins. Cells are stimulated, in the presence or absence of an inhibitor, to trigger endogenous kinase activity and phosphorylation of the substrate. The phosphorylation status of the GFP substrate is detected after cell lysis by addition of a terbium- (Tb-) labeled phosphospecific antibody via time-resolved Förster resonance energy transfer (TR-FRET) signal between Tb and GFP.[21] We used three phosphorylation readouts to interrogate pathway signaling: AKT (pThr308) for PI3K/PDK1, PRAS40 (pThr246) for AKT, and PRAS40 (pSer183) for mTORC1 activity (Figure 1).

Compounds were incubated with the different cell lines in 10-point dose−response format for 60 min to generate IC_{50} curves. Among all newly synthesized series of 3-ethynyl-1*H*-indazoles (**6**−**19**), we found that compounds **6**, **10**, and **13** inhibited both AKT and PRAS40 phosphorylation, while compound **9** inhibited only AKT phosphorylation, with potencies in the low micromolar range (Table 1).

To understand if the inhibition of AKT phosphorylation at Thr308 was a result of a direct inhibition of PDK1 or PI3K, we performed a cell-free kinase assay against both kinases. All of the compounds which displayed inhibition in cell-based assays (**6**, **9**, **10**, **13**) resulted in being active against both kinases, with the highest potency for **10** (IC_{50} = 361 nM) against PI3Kα. Similarly, we tested the compounds against mTOR through a biochemical assay. Compounds **6** and **10** are multiple PI3Kα/PDK1/mTOR inhibitors, while compounds **9** and **13** are dual PI3Kα /PDK1 inhibitors (Table 1). All compounds tested were inactive against AKT as measured by a biochemical kinase assay for AKT1 (data not shown). Further *in vitro* displacement assays against the PI3K isoforms revealed that compounds **6**, **10**, and **13** are α-isoform specific and ATP competitive with about 100-fold selectivity over the β- and γ-isoforms (Table 2).

In order to rationalize the affinity observed for the lead structure **10**, we studied its binding mode within the ATP-binding site of PI3Kα by using computational docking studies. A target binding pocket was derived from the X-ray crystal structure of the ternary complex involving the most common mutant of PI3K catalytic domain p110α (H1047R), its regulatory subunit (p85α), and the drug wortmannin (PDB id: 3hhm).[24] From the docked binding pose, compound **10** appears to be deeply inserted in the ATP-binding site (Figure 2A): the N-2 atom of compound **10** seems to be involved in hydrogen-bonding interactions with the OH of Tyr836 and the indazole moiety further stabilized via hydrogen bond contacts between the NH-1 and the N-2 of the heterocycle with the backbone carbonyl of Asp810 and the backbone NH of Asp933, respectively (Figure 2B). Furthermore, the compound binds to the hinge region of the kinase via a hydrogen bond between the protonated NH of the pyridine ring and the backbone carbonyl of Val851 (Figure 2). From these studies it became apparent that compounds of this series capable of interacting with the hinge region are most effective against PI3Kα. Indeed, the isomer **9**, whose protonated nitrogen could still constitute a suitable hydrogen-bonding donor group interacting with the hinge residue Val851, showed good potency (IC_{50} = 1.85 μM); in compounds **6** and **13**, where the ethynylindazole moiety is linked to an aniline, is the amino group at the 3- or 4-position on the phenyl ring to be involved in the hydrogen bond with the backbone carbonyl of Val851. Indeed, they both showed a low micromolar inhibition (IC_{50} values of 1.05 and 5.12 μM, respectively).

The shift of the amino group at the 2-position on the phenyl ring (**16**) does not allow the compound to form the critical

Table 1. Kinase and Cell-Based Assay Results for Compounds **6**−**21**[a]

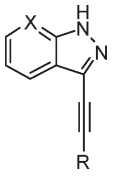

compd ID	R	X	Kinase assay IC_{50} (μM)			Cell-based Assay[d] IC_{50} (μM)		Cell-based Assay GI_{50} (μM)			
			PI3Kα[b]	mTOR[b]	PDK1[c]	AKT [pT308]	PRAS40 [pS183]	PC3	MDA-MB-231	MCF7	Hela
6		CH	1.05	4.97	39.20	17.09	10.80	2.51	8.28	3.23	3.60
7		CH	>100	>100	>50	>100	>50	ND	ND	ND	ND
8	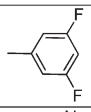	CH	>100	>100	>100	>100	>200	ND	ND	ND	ND
9		CH	1.85	>100	20.80	23.5	>50	6.81	10.48	3.66	5.21
10		CH	0.36	10.70	3.87	12.85	13.60	2.43	7.84	2.58	2.53
11	$-CH_2N(CH_3)_2$	CH	>50	>100	>100	>100	>50	ND	ND	ND	ND
12		CH	>100	>100	>25	>100	>50	ND	ND	ND	ND
13		CH	5.12	>100	12.60	12.90	5.10	2.84	8.29	10.39	5.21
14		CH	>100	>100	>100	>50	>50	ND	ND	ND	ND
15		CH	>100	>100	>100	>50	>50	ND	ND	ND	ND
16		CH	>100	>100	>100	>100	>50	ND	ND	ND	ND
17	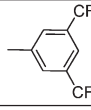	CH	>100	>100	>100	>100	>100	ND	ND	ND	
18		CH	>100	>100	>100	>100	>100	ND	ND	ND	
19	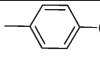	CH	>100	>100	>100	>50	>50	ND	ND	ND	
20		N	3.05	>10	>50	ND	19.1	ND	ND	ND	
21		N	9.0	5.0	>50	ND	>10	ND	ND	ND	

[a] Values are means of at least three or more experiments with a typical standard deviation of less than ±20%. [b] LanthaScreen Eu kinase binding assay. [c] Z′-LYTE kinase activity assay. [d] LanthaScreen cellular assays in HEK293E cell line; AKT (pThr308) for PI3K/PDK1 readout and PRAS40 (pSer183) for mTORC1 readout. ND: not determined (compound was not tested).

interaction with the hinge region, thus explaining its loss of activity (IC_{50} > 100 μM). As expected, the simple phenyl (**7**), fluorophenyl (**8**), trifluoromethylphenyl (**17**), thiophenyl (**18**), and 4-cyanophenyl (**19**) substitutions on 3-ethynylindazole showed poor activity. Accordingly, aliphatic alkynes such as cyclopentyl (**14**), cyclopropyl (**15**), and *N*,*N*-dimethyl (**11**) were inactive both in the biochemical and cell-based assays (Table 1).

Keeping the pyridine group as the most efficient substituent, we explored possible modifications on the indazole ring (**20** and **21**). Isosteric replacement of the indazole with the pyrazolopyridine ring revealed to be detrimental for PI3Kα inhibition. Indeed, by comparing the most active compound of the 3-ethynylindazole series (**10**, IC_{50} = 361 nM) with the corresponding pyrazolopyridine analogue (**20**, IC_{50} = 3.05 μM), a 10-fold loss of activity was observed, and the same trend was

followed by compound **9** (IC_{50} = 1.85 μM) versus compound **21** (IC_{50} = 9.0 μM). Such decrease in activity is expected given that the additional nitrogen atom is not engaged in hydrogen-bonding interactions in the docked structures of compounds **20** and **21** in the binding pocket of PI3Kα (Supporting Information).

Since the ATP-binding pocket of mTOR is highly homologous to that of PI3K, it is not surprising that some of the compounds inhibit both kinases (Table 1). Indeed, even previously reported selective PI3K inhibitors show some degree of activity against mTOR.[16] However, noteworthy compound **10** in our cellular and biochemical assays inhibits also the less structurally related PDK-1. Inhibition of multiple kinases on the PI3K pathway may be highly desirable to suppress oncogenic transformations that result from the activation of the pathway in cancer cells.

To evaluate the drug likeness of the proposed series on empirical ground,[25,26] we gathered information about physicochemical properties of the compounds, such as solubility, cell permeability, and ligand efficiency indices,[27−29] as well as plasma and microsomal stability (Table 3 and Supporting Information). Hence, investigation of these parameters suggests that the compounds of this novel scaffold series may be deemed suitable as lead candidates for further drug optimizations.[30]

On the basis of their cellular efficacy and favorable biopharmaceutical properties, we further investigated the antiproliferative activity of the most promising compounds (**6**, **9**, **10**, and **13**) against human cancer cell lines including prostatic (PC3), breast (MD-MA-231 and MCF7), and cervical (HeLa) cancers. The results are summarized in Table 1. The antitumor activity of compound **10**, which displayed the highest cellular potency inhibiting PI3Kα, mTOR, and PDK1, has been further evaluated against growth/proliferation of the glioblastoma U87 cell line when tested in three-dimensional cultures. The three-dimensional cell culture system has been chosen because it better recapitulates real human tissue with respect to oxygen and nutrient levels, cell−cell contacts, and cellular architecture compared with conventional two-dimensional cell culture systems.[31] It has also been observed that spheroid cultures exhibit

Scheme 1. Synthetic Scheme for Compounds **6**−**21**[a]

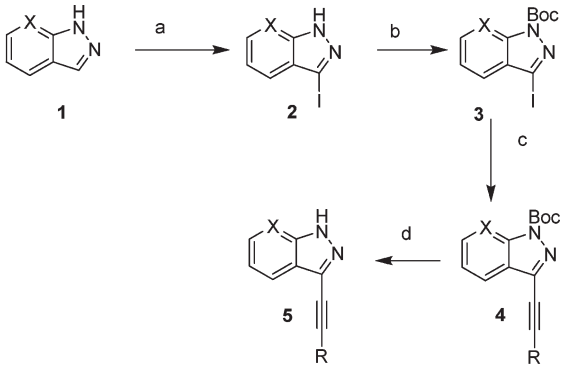

R = aryl or alkyl, see Table 1
X= CH (**1-19**) or N (**20-21**)

[a] Reagents and conditions: (a) iodine, KOH, DMF, room temperature; (b) di-*tert*-butyl dicarbonate, Et_3N, DMAP, CH_3CN, room temperature; (c) aryl or aliphatic alkyne, $Pd(Ph_3P)_2Cl_2$, CuI, Et_3N, CH_3CN, room temperature; (d) TFA, CH_2Cl_2, room temperature.

Table 2. Biochemical Selectivity Profile against PI3K Isoforms, IC_{50} (μM)

compd ID	PI3Kα[a]	PI3Kγ[a]	PI3Kδ[a]
6	1.05	> 100	> 100
10	0.323	40	39
13	5.12	> 100	> 100

[a] These assays were conducted by Invitrogen's SelectScreen Biochemical Kinase (SSBK) Profiling Service. Values are means of at least three or more experiments with a typical standard deviation of less than ±20%.

Table 3. Ligand Efficiency Indices and *in Vitro* ADME Properties of **10** and **13**[a]

parameter		**10**	**13**
ligand efficiency	LE (kcal mol^{-1})	0.5	0.4
binding efficiency index	BEI	29.4	22.7
surface binding efficiency index	SEI	17.5	10.5
lipophilic ligand efficiency	LLE	4.2	2.5
microsomal stability	$t_{1/2}$ (min)	35	> 60
plasma stability	% remaining after 60 min	97	100

[a] Key: LE, ligand efficiency;[28] BEI, binding efficiency index;[27] SEI, surface efficiency index;[27] LLE, lipophilic ligand efficiency indices.[27−29]

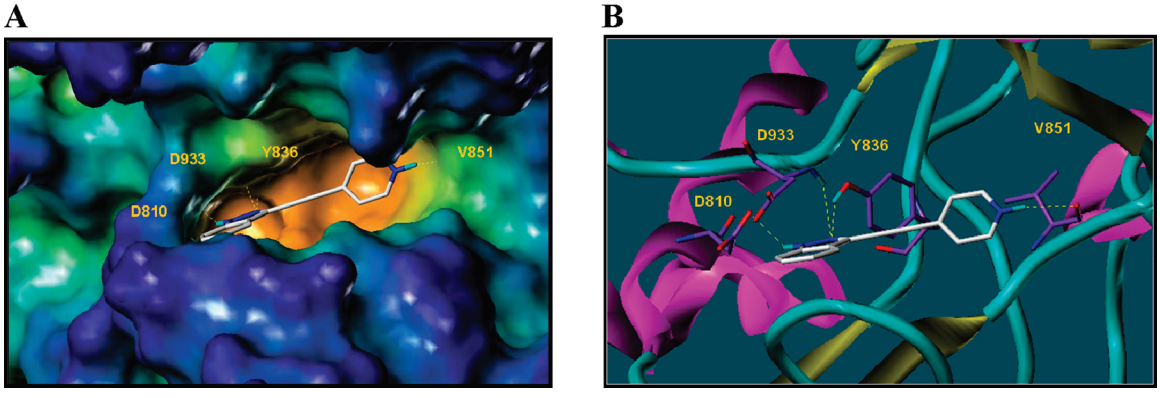

Figure 2. Docking studies of compound **10** within the ATP-binding site of PI3Kα (H1047R) mutant (PDB id: 3hhm).[24] (A) Surface representation of the active site of p110α with the ATP mimic compound **10**. Surface generated with MOLCAD[37] and color coded according to cavity depth (blue, shallow; yellow, deep). Protein residues involved in hydrogen bonds are highlighted. (B) Ribbon representation of the PI3Kα (H1047R) mutant in complex with compound **10** in the same binding pose of (A). Protein residues involved in hydrogen bonds shown as capped sticks.

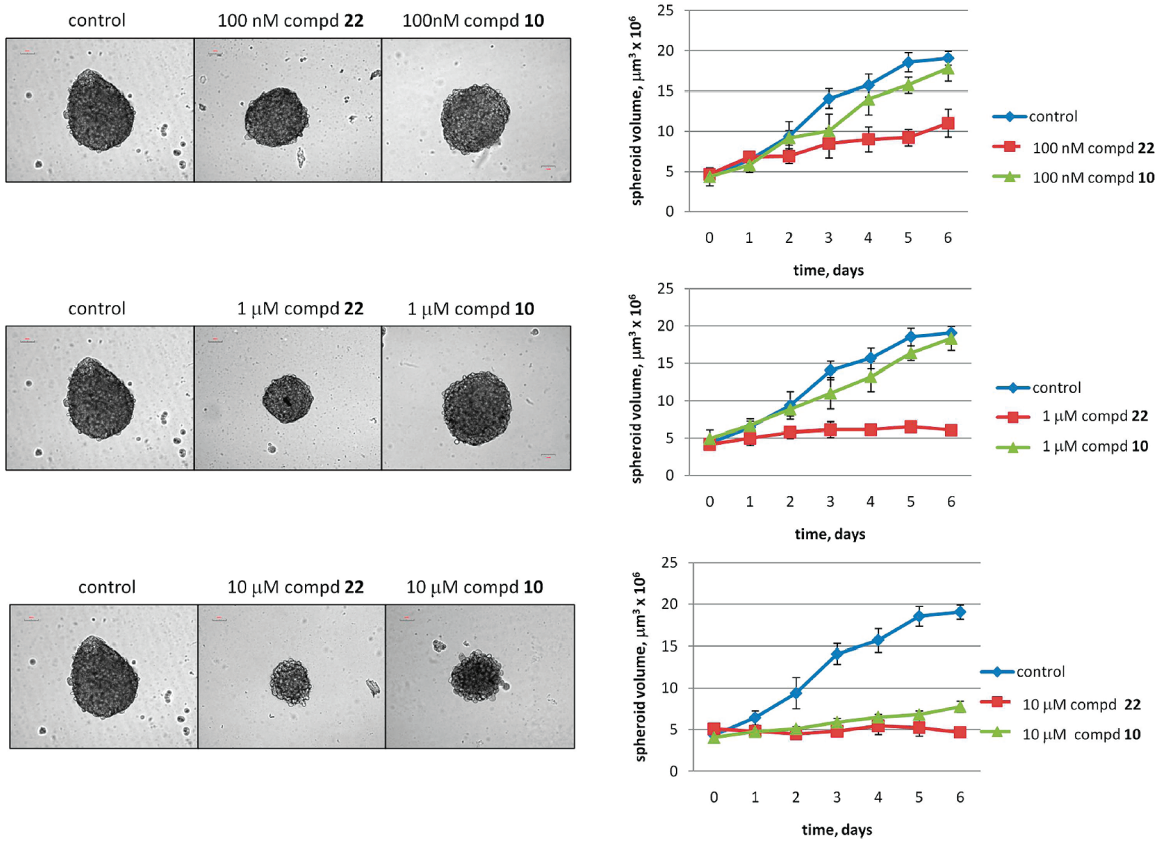

Figure 3. U87 cells grown as spheroids generated by the hanging drop method[34] and treated with the indicated concentration of **22** or compound **10** every day for a total of 6 days. Left panel: Phase-contrast photos representative of four independent experiments. Right panel: Spheroid length and width (measured with an optical micrometer) were used to calculate spheroid volumes (μm^3).

differential sensitivity to known chemotherapeutic agents, as reported for the wortmannin derivative PX-866 (**22**)[32] which showed higher potency in multicellular 3D system than in monolayer.[33] We chose U87 glioblastoma cells because they exhibit deregulated PI3K signaling due to the functional loss of the tumor suppressor PTEN (Figure 1). U87 spheroids, generated through the previously reported hanging drop method,[34] were treated daily, for a total of 6 days, with compounds **10** and **22** as control at different concentrations (Figure 3). Treatment with 10 μM compound **10** every day strongly suppressed cell growth/proliferation, as proved by detected spheroid volumes, comparable to those produced by the potent PI3K inhibitor **22** (Figure 3).

In summary, we successfully developed a useful synthetic route to obtain 3-ethynylindazole derivatives which lead to the identification of a multiple PI3K/PDK1/mTOR inhibitor, with a nanomolar inhibition against PI3Kα. Other indazoles were recently reported as possible inhibitors of other protein kinases;[35] however, the scaffolds reported here, in particular compound **10**, represent a novel and valuable starting point for the development of inhibitors of the PI3K pathway and potentially other kinases (see below). Moreover, due to the observed drug likeness and *in vitro* ADME properties of this novel scaffold (Table 3), we anticipate that further selective and/or multikinase inhibitors could arise from further derivatization of this novel ATP mimetic. In fact, preliminary selectivity panels with compound **10** against 314 protein kinases (Supporting Information) reveal that less than 10% of these proteins showed $\geq$50% inhibition at 10 μM (Table 4). Hence, based on these data, we envision that further elaborations of compound **10** could lead to further selective or multikinase inhibitors against a variety of drug targets.

Table 4. Kinases Which Showed an Inhibition Higher than 50% at 10 μM Concentration of Compound **10**

kinases tested	kinases tested
ABL1 T3151I	MARK4
CDK5/p25	MELK
CHUK (IKK alpha)	MINK1
CLK2	MUSK
DNA-PK	MYLK2 (skMLCK)
FLT3	NTRK1 (TRKA)
FLT3 D835Y	NTRK2 (TRKB)
FLT4 (VEGFR3)	NTRK3 (TRKC)
GSG2 (Haspin)	NUAK1 (ARK5)
IRAK1	PDGFRA T674I
JNK1 (MAPK8)	PDGFRA V561D
JNK2 (MAPK9)	RET V804L
KDR (VEGFR2)	RET Y791F
LRKK2	SGK (SGK1)
LRRK2 G2019S	SYK
MAP4K4 (HGK)	

Experimental Section

Chemistry. Unless otherwise indicated, all anhydrous solvents were commercially obtained and stored in Sure-seal bottles under nitrogen. All other reagents and solvents were purchased as the highest grade available and used without further purification. Thin-layer chromatography (TLC) analysis of reaction mixtures was performed using Merck silica gel 60 F254 TLC plates and visualized using ultraviolet light. NMR

spectra were recorded on Varian 300 or 500 MHz instruments. Chemical shifts (δ) are reported in parts per million (ppm) referenced to ^{1}H (Me_4Si at 0.00). Coupling constants (J) are reported in hertz throughout. Mass spectral data were acquired on a Shimadzu LCMS-2010EV for low resolution and on an Agilent ESI-TOF for either high or low resolution. Purity of all compounds was obtained in a HPLC Breeze from Waters Co. using an Atlantis T3 3 μm 4.6 × 150 mm reverse-phase column. The eluant was a linear gradient with a flow rate of 1 mL/min from 95% A and 5% B to 5% A and 95% B in 15 min followed by 5 min at 100% B (solvent A, H_2O with 0.1% TFA; solvent B, acetonitrile with 0.1% TFA). The compounds were detected at $\lambda = 254$ nm. Purity of key compounds was established by elemental analysis as performed on a Perkin-Elmer series II-2400 and HPLC analysis and determined to be >95%. Combustion analysis was performed by NuMega Resonance Laboratories, San Diego, CA, USA.

Synthesis of *tert*-Butyl 3-(Phenylethynyl)-1*H*-indazole-1-carboxylate (4, R = Ph). To a solution of compound **3** (343 mg, 1 mmol) in CH_3CN (5 mL) were added phenyl acetylene (0.13 mL, 1.2 mmol), CuI (20 mg, 0.10 mmol), $Pd(Ph_3P)_2Cl_2$ (70 mg, 0.10 mmol), and Et_3N (0.42 mL, 3 mmol), respectively, at room temperature under nitrogen atmosphere. The reaction mixture was stirred at room temperature for 16 h; then solvent was removed *in vacuo*. The residue was chromatographed over silica gel (2% ethyl acetate in hexane) to give a Boc-protected product **4** (270 mg, 85%).

Synthesis of 3-(Phenylethynyl)-1*H*-indazole (7). To a solution of **4** (150 mg, 0.47 mmol) in CH_2Cl_2 (3 mL) was added TFA (1 mL) at room temperature. The resulting mixture was stirred at room temperature for 3 h; then solvent and TFA were removed *in vacuo*. The residue was extracted with CH_2Cl_2 (50 mL), washed with saturated $NaHCO_3$ aqueous solution (3 × 30 mL) and brine (30 mL), dried ($MgSO_4$), and concentrated *in vacuo*. The residue was chromatographed over silica gel (40% ethyl acetate in hexane) to afford a white solid compound **7** (94 mg, 92%). ^{1}H NMR (300 MHz, $CDCl_3$) δ 7.26−7.34 (m, 1H), 7.40−7.50 (m, 5H), 7.66−7.76 (m, 2H), 7.95 (d, J = 7.8 Hz, 1H), 11.68 (br s, 1H, NH); MS m/z 219 $(M + H)^+$, 166, 155, 121, 88; HRMS calcd for $C_{15}H_{11}N_2$ 219.0917 (M H), found 219.0918.

Following the above-mentioned procedure and the use of the appropriate starting materials and reagents, compounds **6**−**16** were prepared. Yields refer to the final deprotection step.

Synthesis of 4-((1*H*-Indazol-3-yl)ethynyl)aniline (6). Yield 65%; ^{1}H NMR (300 MHz, CD_3OD) δ 5.24 (br s, 2H, NH_2), 6.57−6.60 (m, 2H), 7.12−7.15 (m, 1H), 7.24 (d, J = 7.5 Hz, 2H), 7.28−7.46 (m, 2H), 7.70 (d, J = 6.9 Hz, 1H), 11.82 (br s, 1H, NH); MS m/z 234 $(M + H)^+$, 158, 149, 121, 102, 65; HRMS calcd for $C_{15}H_{12}N_3$ 234.1031 (M + H), found 234.1021.

Synthesis of 3-((3,5-Difluorophenyl)ethynyl)-1*H*-indazole (8). Yield 89%; ^{1}H NMR (300 MHz, DMSO) δ 7.27 (t, J = 7.5 Hz, 1H), 7.36−7.51 (m, 4H), 7.63 (d, J = 8.4 Hz, 1H), 7.92 (d, J = 8.1 Hz, 1H), 13.32 (br s, 1H); MS m/z 255 $(M + H)^+$, 149, 121; HRMS calcd for $C_{15}H_9F_2N_2$ 255.0728 (M + H), found 255.0726.

Synthesis of 3-(Pyridin-3-ylethynyl)-1*H*-indazole (9). Yield 92%; ^{1}H NMR (300 MHz, $CDCl_3$) δ 7.24−7.41 (m, 3H), 7.46 (m, 1H), 7.59 (d, J = 7.8 Hz, 1H), 7.87−7.99 (m, 2H), 8.63 (s, 1H), 11.32 (br s, 1H, NH); MS m/z 220 $(M + H)^+$, 192, 121, 102; HRMS calcd for $C_{14}H_{10}N_3$ 220.0875 (M + H), found 220.0877.

Synthesis of 3-(Pyridin-4-ylethynyl)-1*H*-indazole (10). Yield 91%; ^{1}H NMR (400 MHz, DMSO) δ 7.29 (t, J = 7.3 Hz, 1H), 7.45 (t, J = 7.3 Hz, 1H), 7.62−7.67 (m, 3H), 7.89 (d, J = 7.9 Hz, 1H), 8.65 (d, J = 6.1 Hz, 2H), 13.68 (br s, 1H, NH); HRMS calcd for $C_{14}H_{10}N_3$ 220.0875 (M + H), found 220.0878. Anal. Calcd for $C_{14}H_9N_3$: C, 76.70; H, 4.14; N, 19.17. Found: C, 76.58; H, 4.29; N, 19.01.

Synthesis of 3-(1*H*-Indazol-3-yl)-*N*,*N*-dimethylprop-2-yn-1-amine (11). Yield 90%; ^{1}H NMR (300 MHz, $CDCl_3$) δ 2.47 (s, 6H), 3.67 (s, 2H), 7.18−7.27 (m, 1H), 7.40 (t, J = 7.6 Hz, 1H), 7.56 (d, J = 8.4 Hz, 1H), 7.65 (d, J = 7.8 Hz, 1H), 11.65 (br s, 1H, NH); MS m/z 200 $(M + H)^+$, 155, 127, 83; HRMS calcd for $C_{12}H_{14}N_3$ 200.1182 (M + H), found 200.1190.

Synthesis of 3-(Pyridin-2-ylethynyl)-1*H*-indazole (12). Yield 91%; ^{1}H NMR (300 MHz, CD_3OD) δ 7.29 (t, J = 6.9 Hz, 1H), 7.40−7.55 (m, 2H), 7.60 (d, J = 8.1 Hz, 1H), 7.77 (d, J = 6.6 Hz, 2H), 7.93 (d, J = 6.9 Hz, 2H), 11.31 (br s, 1H, NH); HRMS calcd for $C_{14}H_{10}N_3$ 220.0875 (M + H), found 220.0878.

Synthesis of 3-((1*H*-Indazol-3-yl)ethynyl)aniline (13). Yield 91%; ^{1}H NMR (300 MHz, CD_3OD) δ 5.26 (br s, 2H, NH_2), 6.76 (d, J = 7.8 Hz, 1H), 6.94 (d, J = 7.5 Hz, 1H), 6.97 (s, 1H), 7.13 (t, J = 8.1 Hz, 1H), 7.24 (t, J = 8.1 Hz, 1H), 7.44 (t, J = 8.1 Hz, 1H), 7.56 (d, J = 7.8 Hz, 1H), 7.84 (d, J = 8.7 Hz, 1H), 11.32 (br s, 1H, NH); HRMS calcd for $C_{15}H_{12}N_3$ 234.1031 (M + H), found 234.1025. Anal. Calcd for $C_{15}H_{11}N_3$: C, 77.23; H, 4.75; N, 18.01. Found: C, 77.01; H, 4.89; N, 17.89.

Synthesis of 3-(Cyclopentylethynyl)-1*H*-indazole (14). Yield 92%; ^{1}H NMR (300 MHz, $CDCl_3$) δ 1.66−1.69 (m, 2H), 1.80−189 (m, 4H), 2.02−2.19 (m, 2H), 2.94−3.08 (m, 1H), 7.22 (t, J = 7.4 Hz, 1H), 7.41 (t, J = 7.4 Hz, 1H), 7.70 (d, J = 7.8 Hz, 1H), 7.82 (d, J = 7.8 Hz, 1H), 11.84 (br s, 1H, NH); HRMS calcd for $C_{14}H_{15}N_2$ 211.1235 (M + H), found 211.1233.

Synthesis of 3-(Cyclopropylethynyl)-1*H*-indazole (15). Yield 90%; ^{1}H NMR (300 MHz, $CDCl_3$) δ 0.92−1.00 (m, 4H), 1.56−1.67 (m, 1H), 7.17−7.27 (m, 1H), 7.36−7.46 (m, 1H), 7.66 (d, J = 8.4 Hz, 1H), 7.82 (d, J = 8.1 Hz, 1H), 9.86 (br s, 1H, NH); HRMS calcd for $C_{12}H_{11}N_2$ 183.0922 (M + H), found 183.0925.

Synthesis of 2-((1*H*-Indazol-3-yl)ethynyl)aniline (16). Yield 81%; ^{1}H NMR (300 MHz, CD_3OD) δ 5.26 (br s, 2H, NH_2), 6.58−6.60 (m, 2H), 7.12−7.15 (m, 1H), 7.24 (d, J = 7.5 Hz, 2H), 7.28−7.46 (m, 2H), 7.70 (d, J = 6.9 Hz, 1H), 11.80 (br s, 1H, NH); MS m/z 234 $(M + H)^+$, 158, 149, 121, 102, 65; HRMS calcd for $C_{15}H_{12}N_3$ 234.1031 (M + H), found 234.1021.

Synthesis of 3-((3,5-Bis(trifluoromethyl)phenyl)ethynyl)-1*H*-indazole (17). Yield 90%; ^{1}H NMR (300 MHz, $CDCl_3$) δ 7.32 (t, J = 8.5 Hz, 1H), 7.49 (t, J = 6.6 Hz, 1H), 7.85−7.94 (m, 2H), 8.07 (s, 2H), 9.56 (br s, 1H, NH); MS m/z 355 $(M + H)^+$, 275, 244, 149, 130, 127, 121, 118, 88; HRMS calcd for $C_{17}H_9F_6N_2$ 355.0664 (M + H), found 355.0664.

Synthesis of 3-(Thiophen-3-ylethynyl)-1*H*-indazole (18). Yield 92%; ^{1}H NMR (300 MHz, $CDCl_3$) δ 7.22−7.46 (m, 4H), 7.63−7.70 (m, 2H), 7.90 (d, J = 8.1 Hz, 1H), 9.52 (br s, 1H, NH); MS m/z 225 $(M + H)^+$, 130, 121, 102; HRMS calcd for $C_{13}H_9N_2S$ 225.0481 (M + H), found 225.0484.

Synthesis of 4-((1*H*-Indazol-3-yl)ethynyl)benzonitrile (19). Yield 91%; ^{1}H NMR (300 MHz, CD_3OD) δ 7.28 (t, J = 7.5 Hz, 1H), 7.47 (t, J = 7.8 Hz, 1H), 7.59 (d, J = 8.1 Hz, 1H), 7.74−7.76 (m, 4H), 7.85 (d, J = 8.1 Hz, 1H), 10.89 (br s, 1H, NH); MS m/z 244 $(M + H)^+$, 217, 149, 141, 130, 127, 121, 102; HRMS calcd for $C_{16}H_{10}N_3$ 244.0869 (M + H), found 244.0875.

Synthesis of 3-(Pyridin-4-ylethynyl)-1*H*-pyrazolo[3,4-*b*]pyridine (20). Yield 86%; ^{1}H NMR (300 MHz, DMSO-d_6) δ 7.37 (dd, J = 8.1 and 4.5 Hz, 1H), 7.65−7.69 (m, 2H), 8.42 (dd, J = 8.1 and 1.2 Hz, 1H), 8.65 (dd, J = 4.5 and 1.2 Hz, 1H), 8.67−8.71 (m, 2H), 13.89 (br s, 1H, NH); MS m/z 221 $(M + H)^+$, 159, 130, 121, 102, 88, 85, 56; HRMS calcd for $C_{13}H_9N_4$ (M + H) 221.0827, found 221.0822.

Synthesis of 3-(Pyridin-2-ylethynyl)-1*H*-pyrazolo[3,4-*b*]pyridine (21). Yield 83%; ^{1}H NMR (300 MHz, DMSO-d_6) δ 7.35 (dd, J = 8.1 and 4.2 Hz, 1H), 7.42 (t, J = 5.7 Hz, 1H), 7.79 (d, J = 7.5 Hz, 1H), 7.90 (t, J = 7.7 Hz, 1H), 8.35 (d, J = 8.1 Hz, 1H), 8.60−8.67 (m, 2H), 13.87 (br s, 1H, NH); HRMS calcd for $C_{13}H_9N_4$ (M + H) 221.0827, found 221.0824.

Assays. LanthaScreen Cellular Assay. Cell-based assays for both AKT and PRAS40 phosphorylation were carried out using LanthaScreen cellular assay technology from Invitrogen (Carlsbad, CA).[21] Briefly, the assay protocol for compound screening is as follows. Cells were plated in white tissue culture-treated 384-well assay plates at a density of 20000 cells per well in 32 μL of assay medium (low glucose DMEM+0.1% bovine serum albumin, BSA).

After overnight serum starvation, cells were pretreated with 4 μL of compound at the indicated concentrations (10-point dose−response in duplicate) for 60 min. The cells were then stimulated with insulin (EC_{80} concentration of ~5 ng/mL) for 30 min to activate PI3K/AKT/mTOR signaling. The assay medium was subsequently removed via aspiration, and cells were lysed by the addition of 20 μL of LanthaScreen cellular assay lysis buffer supplemented with protease and phosphatase inhibitor cocktails (Sigma P8340 and P2850, respectively) as well as 2 nM Tb-labeled detection antibody, also from Invitrogen. Following 2 h assay equilibration at room temperature, the TR-FRET emission ratios were acquired on a PerkinElmer EnVision fluorescence plate reader (Waltham, MA) with TRF laser excitation and emission wavelengths of 520 and 495 nm. Data analysis and curve fitting were performed using XLfit4 and GraphPad Prism4 software.

PI3Kα *in Vitro* Assay. The lipid kinase PI3K was assayed by using a LanthaScreen Eu kinase binding assay technology from Invitrogen. To a solution of the compounds diluted in assay buffer (25 mM Tris-HCl, 5 mM $MgCl_2$, 0.02% CHAPS) were added the following components: the kinase tracer (PV6088, 20 nM final concentration), the kinase PIK3CA/PIK3R1 (PV4788, 5 nM final concentration), and Eu-labeled anti-His tag antibody (PV6089, 2 nM final concentration).

The assay was performed in Corning 3673 white 384-well assay plates. Following 1 h assay equilibration at room temperature, the TR-FRET emission ratios were acquired on a PerkinElmer EnVision fluorescence plate reader (Waltham, MA) with TRF laser excitation and emission wavelengths of 665 and 615 nm. Data analysis and curve fitting were performed using XLfit4 and GraphPad Prism4 software.

mTOR *in Vitro* Assay. Mammalian target of rapamycin (mTOR) was assayed by using a LanthaScreen Eu kinase binding assay technology from Invitrogen. To a solution of the compound diluted in assay buffer (25 mM Tris-HCl, 5 mM $MgCl_2$, 0.02% CHAPS) were added the following components: the kinase tracer (PV6087, 20 nM final concentration), the kinase FRAP1 (PV4753, mTOR, 5 nM final concentration), and Eu-labeled anti-GST tag antibody (PV5594, 2 nM final concentration).

The assay was performed in Corning 3673 white 384-well assay plates. Following 1 h assay equilibration at room temperature, the TR-FRET emission ratios were acquired on a PerkinElmer EnVision fluorescence plate reader (Waltham, MA) with TRF laser excitation and emission wavelengths of 665 and 615 nm. Data analysis and curve fitting were performed using XLfit4 and GraphPad Prism4 software.

PDK1 *in Vitro* Assay. The PDK1 kinase was tested by using the Z′-LYTE biochemical assay technology from Invitrogen (PV 3180). The assay was performed in Corning 3676 black 384-well assay plates. The final 10 μL of the kinase reaction consisted of 9.75−49.4 ng of PDK1 and 2 μM substrate Ser/Thr 07 in 50 mM of HEPES buffer at pH 8.0, containing 0.01% BRIJ-35, 10 mM $MgCl_2$, 1 mM EGTA, and 0.01% NaN_3. ATP concentration at the K_m value was used. After the 1 h kinase reaction incubation, 5 μL of a 1:32768 dilution of development reagent A was added. After the development reaction, where a site-specific protease recognizes and cleaves the nonphosphorylated peptide, a ratiometric read-out of the donor emission (coumarin, 445 nm) over the acceptor (fluorescein, 520 nm) was detected by a PerkinElmer EnVision fluorescence plate reader (Waltham, MA). Data analysis and curve fitting were performed using XLfit4 and GraphPad Prism4 software.

Antiproliferative Assay. All human cancer cell lines were obtained from the American Type Culture Collection (Manassas, VA, USA) and were maintained in 5% CO_2 at 37 °C. Human cervical carcinoma (HeLa) and U87 glioblastoma cells were grown in Dulbecco's modified Eagle's medium (DMEM; Cellgro) supplemented with 10% fetal bovine serum (FBS; Omega Scientific) and 1% penicillin/streptomycin (Omega Scientific). MDA-MB-231 and MCF7 breast cancer cells and PC3 prostate cancer cells were cultured in RPMI plus GlutaMAX medium (Gibco) plus 10% FBS and 1% penicillin/streptomycin.

Approximately 3000 cells were seeded into individual wells of a 96-well tissue culture plate and incubated for 24 h. Cells were replenished with fresh medium (0.1 mL/well) and exposed to triplicates of different concentration solutions (from 0.5 to 100 μM) of test compounds. The analyzed inhibitors were dissolved in DMSO reaching a final DMSO concentration of 0.5%. After incubation for 72 h at 37 °C and 5% CO_2, cell viability was assessed using ATPlite assay from Perkin-Elmer (Waltham, MA). Viability was normalized to control cells which were treated with the vehicle, DMSO. The reported IG_{50} values were calculated by Prism5 (GraphPad).

3D Culture Assay. U87 cells were induced to form spheroids via a hanging drop method.[34] Cells were plated at 200 cells per well (20 μL) of a Nunc-60 well microwell MiniTray (polystyrene). The trays were covered, inverted, and placed in a humidity chamber for 5 days until one spheroid formed in each well. The spheroids were then transferred into a 48-well plate coated in 1% low melting point agarose to prevent them from adhering. The spheroids were measured, and DMSO or drug was added every 24 h for 6 days. Spheroid length and width (measured with an optical micrometer) were used to calculate spheroid volumes (μm^3).

Microsomal Stability Assay (Rat Liver Microsome Assay). Test compound solutions were incubated with rat liver microsomes (RLM) for 60 min at 37.5 °C. The final incubation solutions contained 4 μM test compound, 2 mM NADPH, 1 mg/mL (total protein) microsomes, and 50 mM phosphate (pH 7.2). Compound solutions, protein, and phosphate were preincubated at 37.5 °C for 5 min, and the reactions were initiated by the addition of NADPH and incubated for 1 h at 37.5 °C. Aliquots were taken at 15 min time points and quenched with the addition of methanol containing internal standard. Following protein precipitation and centrifugation, the samples were analyzed by LC-MS. Test compounds were run in duplicate with two control compounds of known half-life.

Plasma Stability Assay. Test compound solution was incubated (1 μM, 2.5% final DMSO concentration) with fresh rat plasma at 37 °C. The reactions were terminated at 0, 30, and 60 min by the addition of 2 volumes of methanol containing internal standard. Following protein precipitation and centrifugation, the samples were analyzed by LC-MS. The percentage of parent compound remaining at each time point relative to the 0 min sample is calculated from peak area ratios in relation to the internal standard. Compounds were run in duplicate with a positive control known to be degraded in plasma.

Molecular Modeling. Molecular modeling studies were conducted on a Linux workstation and a 64 3.2-GHz CPUs Linux cluster. Docking studies were performed using the X-ray coordinates of the p110alpha (H1037R) mutant in complex with niSH2 of p85alpha and the drug wortmannin (PDB id: 3hhm).[24] The PI3Kα crystal structure was extracted from the Protein Data Bank, and the complexed ligand was used to define the binding site for docking of small molecules. The genetic algorithm (GA) procedure in the GOLD docking software performed flexible docking of small molecules whereas the protein structure was static.[36−38] For each compound, 20 solutions were generated and subsequently ranked according to GoldScore. Molecular surfaces were generated with MOLCAD[38] and docked structures analyzed with Sybyl (Tripos Inc., St. Louis, MO).

Acknowledgment. We gratefully acknowledge financial support from the NIH (Grant P01CA128814 to M.P.).

Supporting Information Available: A list of 314 kinases used for the selectivity profile, graphs reporting plasma and microsomal stability of compounds **10** and **13**, and docking studies with compound **20**. This material is available free of charge via the Internet at http://pubs.acs.org.

References

(1) Datta, S. R.; Dudek, H.; Tao, X.; Masters, S.; Fu, H.; Gotoh, Y.; Greenberg, M. E. Akt phosphorylation of BAD couples survival signals to the cell-intrinsic death machinery. *Cell* **1997**, *91*, 231–241.

(2) Frame, S.; Cohen, P. GSK3 takes centre stage more than 20 years after its discovery. *Biochem. J.* **2001**, *359*, 1–16.

(3) Kandel, E. S.; Skeen, J.; Majewski, N.; Di Cristofano, A.; Pandolfi, P. P.; Feliciano, C. S.; Gartel, A.; Hay, N. Activation of Akt/protein kinase B overcomes a G(2)/m cell cycle checkpoint induced by DNA damage. *Mol. Cell. Biol.* **2002**, *22*, 7831–7841.

(4) Shaw, R. J.; Cantley, L. C. Ras, PI(3)K and mTOR signalling controls tumour cell growth. *Nature* **2006**, *441*, 424–430.

(5) Carnero, A.; Blanco-Aparicio, C.; Renner, O.; Link, W.; Leal, J. F. M. The PTEN/PI3K/AKT signalling pathway in cancer, therapeutic implications. *Curr. Cancer Drug Targets* **2008**, *8*, 187–198.

(6) Chiang, G. G.; Abraham, R. T. Targeting the mTOR signaling network in cancer. *Trends Mol. Med.* **2007**, *13*, 433–442.

(7) Cicenas, J. The potential role of Akt phosphorylation in human cancers. *Int. J. Biol. Markers* **2008**, *23*, 1–9.

(8) Yuan, T. L.; Cantley, L. C. PI3K pathway alterations in cancer: variations on a theme. *Oncogene* **2008**, *27*, 5497–5510.

(9) Haluska, F. G.; Tsao, H.; Wu, H.; Haluska, F. S.; Lazar, A.; Goel, V. Genetic alterations in signaling pathways in melanoma. *Clin. Cancer Res.* **2006**, *12*, 2301s–2307s.

(10) Cully, M.; You, H.; Levine, A. J.; Mak, T. W. Beyond PTEN mutations: the PI3K pathway as an integrator of multiple inputs during tumorigenesis. *Nat. Rev. Cancer* **2006**, *6*, 184–192.

(11) Samuels, Y.; Wang, Z.; Bardelli, A.; Silliman, N.; Ptak, J.; Szabo, S.; Yan, H.; Gazdar, A.; Powell, S. M.; Riggins, G. J.; Willson, J. K. V.; Markowitz, S.; Kinzler, K. W.; Vogelstein, B.; Velculescu, V. E. High frequency of mutations of the PIK3CA gene in human cancers. *Science* **2004**, *304*, 554.

(12) Maira, S.-M.; Stauffer, F.; Brueggen, J.; Furet, P.; Schnell, C.; Fritsch, C.; Brachmann, S.; Chene, P.; De Pover, A.; Schoemaker, K.; Fabbro, D.; Gabriel, D.; Simonen, M.; Murphy, L.; Finan, P.; Sellers, W.; Garcia-Echeverria, C. Identification and characterization of NVP-BEZ235, a new orally available dual phosphatidylinositol 3-kinase/mammalian target of rapamycin inhibitor with potent in vivo antitumor activity. *Mol. Cancer Ther.* **2008**, *7*, 1851–1863.

(13) Lindsley, C. W.; Barnett, S. F.; Layton, M. E.; Bilodeau, M. T. The PI3K/Akt pathway: recent progress in the development of ATP-competitive and allosteric Akt kinase inhibitors. *Curr. Cancer Drug Targets* **2008**, *8*, 7–18.

(14) Garcia-Echeverria, C.; Sellers, W. R. Drug discovery approaches targeting the PI3K/Akt pathway in cancer. *Oncogene* **2008**, *27*, 5511–5526.

(15) Fasolo, A.; Sessa, C. mTOR inhibitors in the treatment of cancer. *Expert Opin. Invest. Drugs* **2008**, *17*, 1717–1734.

(16) Brachmann, S.; Fritsch, C.; Maira, S.-M.; Garcia-Echeverria, C. PI3K and mTOR inhibitors: a new generation of targeted anticancer agents. *Curr. Opin. Cell Biol.* **2009**, *21*, 194–198.

(17) Engelman, J. A.; Chen, L.; Tan, X.; Crosby, K.; Guimaraes, A. R.; Upadhyay, R.; Maira, M.; McNamara, K.; Perera, S. A.; Song, Y.; Chirieac, L. R.; Kaur, R.; Lightbown, A.; Simendinger, J.; Li, T.; Padera, R. F.; Garcia-Echeverria, C.; Weissleder, R.; Mahmood, U.; Cantley, L. C.; Wong, K.-K. Effective use of PI3K and MEK inhibitors to treat mutant Kras G12D and PIK3CA H1047R murine lung cancers. *Nat. Med.* **2008**, *14*, 1351–1356.

(18) Morphy, R. Selectively nonselective kinase inhibition: striking the right balance. *J. Med. Chem.* **2010**, *53*, 1413–1437.

(19) Serra, V.; Markman, B.; Scaltriti, M.; Eichhorn, P. J. A.; Valero, V.; Guzman, M.; Botero, M. L.; Llonch, E.; Atzori, F.; Di Cosimo, S.; Maira, M.; Garcia-Echeverria, C.; Parra, J. L.; Arribas, J.; Baselga, J. NVP-BEZ235, a dual PI3K/mTOR inhibitor, prevents PI3K signaling and inhibits the growth of cancer cells with activating PI3K mutations. *Cancer Res.* **2008**, *68*, 8022–8030.

(20) Gaitonde, S.; De, S. K.; Tcherpakov, M.; Dewing, A.; Yuan, H.; Riel-Mehan, M.; Krajewski, S.; Robertson, G.; Pellecchia, M.; Ronai, Z. E. BI-69A11-mediated inhibition of AKT leads to effective regression of xenograft melanoma. *Pigment Cell Melanoma Res.* **2009**, *22*, 187–195.

(21) Carlson, C. B.; Robers, M. B.; Vogel, K. W.; Machleidt, T. Development of LanthaScreen cellular assays for key components within the PI3K/AKT/mTOR pathway. *J. Biomol. Screening* **2009**, *14*, 121–132.

(22) De, S. K.; Stebbins, J. L.; Chen, L.-H.; Riel-Mehan, M.; Machleidt, T.; Dahl, R.; Yuan, H.; Emdadi, A.; Barile, E.; Chen, V.; Murphy, R.; Pellecchia, M. Design, synthesis, and structure-activity relationship of substrate competitive, selective, and in vivo active triazole and thiadiazole inhibitors of the c-Jun N-terminal kinase. *J. Med. Chem.* **2009**, *52*, 1943–1952.

(23) Stebbins, J. L.; De, S. K.; Machleidt, T.; Becattini, B.; Vazquez, J.; Kuntzen, C.; Chen, L.-H.; Cellitti, J. F.; Riel-Mehan, M.; Emdadi, A.; Solinas, G.; Karin, M.; Pellecchia, M. Identification of a new JNK inhibitor targeting the JNK-JIP interaction site. *Proc. Natl. Acad. Sci. U.S.A.* **2008**, *105*, 16809–16813.

(24) Mandelker, D.; Gabelli, S. B.; Schmidt-Kittler, O.; Zhu, J.; Cheong, I.; Huang, C.-H.; Kinzler, K. W.; Vogelstein, B.; Amzel, L. M. A frequent kinase domain mutation that changes the interaction between PI3Kalpha and the membrane. *Proc. Natl. Acad. Sci. U.S.A.* **2009**, *106*, 16996–17001.

(25) Hann, M. M.; Oprea, T. I. Pursuing the leadlikeness concept in pharmaceutical research. *Curr. Opin. Chem. Biol.* **2004**, *8*, 255–263.

(26) Oprea, T. I.; Davis, A. M.; Teague, S. J.; Leeson, P. D. Is there a difference between leads and drugs? A historical perspective. *J. Chem. Inf. Comput. Sci.* **2001**, *41*, 1308–1315.

(27) Abad-Zapatero, C.; Metz, J. T. Ligand efficiency indices as guideposts for drug discovery. *Drug Discovery Today* **2005**, *10*, 464–469.

(28) Hopkins, A. L.; Groom, C. R.; Alex, A. Ligand efficiency: a useful metric for lead selection. *Drug Discovery Today* **2004**, *9*, 430–431.

(29) Perola, E. An analysis of the binding efficiencies of drugs and their leads in successful drug discovery programs. *J. Med. Chem.* **2010**, *53*, 2986–2997.

(30) Hajduk, P. J. Fragment-based drug design: how big is too big? *J. Med. Chem.* **2006**, *49*, 6972–6976.

(31) Griffith, L. G.; Swartz, M. A. Capturing complex 3D tissue physiology in vitro. *Nat. Rev. Mol. Cell Biol.* **2006**, *7*, 211–224.

(32) Ihle, N. T.; Williams, R.; Chow, S.; Chew, W.; Berggren, M. I.; Paine-Murrieta, G.; Minion, D. J.; Halter, R. J.; Wipf, P.; Abraham, R.; Kirkpatrick, L.; Powis, G. Molecular pharmacology and antitumor activity of PX-866, a novel inhibitor of phosphoinositide-3-kinase signaling. *Mol. Cancer Ther.* **2004**, *3*, 763–772.

(33) Howes, A. L.; Chiang, G. G.; Lang, E. S.; Ho, C. B.; Powis, G.; Vuori, K.; Abraham, R. T. The phosphatidylinositol 3-kinase inhibitor, PX-866, is a potent inhibitor of cancer cell motility and growth in three-dimensional cultures. *Mol. Cancer Ther.* **2007**, *6*, 2505–2514.

(34) Kelm, J. M.; Timmins, N. E.; Brown, C. J.; Fussenegger, M.; Nielsen, L. K. Method for generation of homogeneous multicellular tumor spheroids applicable to a wide variety of cell types. *Biotechnol. Bioeng.* **2003**, *83*, 173–180.

(35) Poulsen, A.; William, A.; Lee, A.; Blanchard, S.; Teo, E.; Deng, W.; Tu, N.; Tan, E.; Sun, E.; Goh, K. L.; Ong, W. C.; Ng, C. P.; Goh, K. C.; Bonday, Z. Structure-based design of Aurora A & B inhibitors. *J. Comput.-Aided Mol. Des.* **2008**, *22*, 897–906.

(36) Jones, G.; Willett, P.; Glen, R. C.; Leach, A. R.; Taylor, R. Development and validation of a genetic algorithm for flexible docking. *J. Mol. Biol.* **1997**, *267*, 727–748.

(37) Eldridge, M. D.; Murray, C. W.; Auton, T. R.; Paolini, G. V.; Mee, R. P. Empirical scoring functions: I. The development of a fast empirical scoring function to estimate the binding affinity of ligands in receptor complexes. *J. Comput.-Aided Mol. Des.* **1997**, *11*, 425–445.

(38) Teschner, M.; Henn, C.; Vollhardt, H.; Reiling, S.; Brickmann, J. Texture mapping: a new tool for molecular graphics. *J. Mol. Graphics* **1994**, *12*, 98–105.